Integrating sphere simulation: application to total flux scale realization

Y. Ohno

A method is proposed for realizing the total flux scale of light sources by use of an integrating sphere with an opening to introduce a known amount of flux from a luminous intensity standard or a spectral irradiance standard lamp placed outside the sphere. Computer simulations were made on several models of an integrating sphere, designed to compare the total flux of a test lamp inside the sphere with the flux introduced from an external source. I describe the theory and algorithm of the simulation, present the results of the simulation for varying conditions of sphere geometry such as size and location of the baffles, internal source, and wall reflectance, and predict that one of the models has sufficient accuracy to calibrate lamps for total flux.

Key words: Calibration, computer simulation, integrating sphere, lumen, luminous flux, photometer, photometry, radiant flux, ray tracing, scale, standards, total flux.

1. Introduction

The total luminous flux (lumen) is one of the most important measured quantities for light sources. The total luminous flux is usually measured at laboratories in industry by integration of sphere photometers in comparison with standard lamps, whereas the primary standards of the total luminous flux are most often realized at national laboratories by goniophotometers. However, it is not always convenient to build and maintain goniophotometers because they require a large dark room space, a costly high-precision moving mechanism, and long hours of operation. Efforts continue to improve these requirements of goniophotometers as reported recently.[1–3] Also, most goniophotometers need to rotate the lamp to be measured around one axis or more, which may cause another error for lamps that are sensitive to the burning position or drafts.[4,5] The shadow of their lamp-rotating mechanism may also cause an error in the measured total flux, which restricts the type of lamp for flux standards. There is also an increasing need for the spectral total-radiant-flux standards,[6] but such inconveniences with goniophotometers make the spectral measurements even more difficult.

Considering such problems, I investigated an alternative method of realizing the total flux scale at the National Institute of Standards and Technology. This research is an attempt to calibrate the total flux of a lamp inside an integrating sphere against the known amount of flux coming into the sphere from an external source. This new method has the potential of generating a total (luminous or spectral) flux scale through much simpler procedures and with better accuracy. Two models of an integrating sphere have been designed for this purpose. Each model consists of an observation window, an opening to introduce flux from an external source, a baffle between the test lamp and the window, and another baffle between the test lamp and the opening. To evaluate the performance of the sphere models, a theoretical approach has been taken.

General theories of integrating spheres were well established, and various effects in integrating spheres, except for baffles, were analyzed theoretically.[7–10] The effects of a baffle in an integrating sphere were also analyzed theoretically and experimentally.[11–16] Rotter,[13] Brown,[14] and de Visser and Van der Woude[16] obtained the wall illuminance distribution of a sphere with one baffle by numerical solutions of integral equations by utilizing the axial symmetry of the sphere geometry. These approaches, however, cannot be applied to integrating spheres as designed in this research, which include two baffles and two openings located in axial asymmetry. Thus a computer simulation based on the ray-tracing technique has been applied for the integrating-sphere models designed.

First the theory and algorithm of the computer simulation are described. To verify the program,

The author is with the Radiometric Physics Division, National Institute of Standards and Technology, Room A305, Building 220, Gaithersburg, Maryland 20899.

Received 7 June 1993; revised manuscript received 24 September 1993.
0003-6935/94/132637-11$06.00/0.
© 1994 Optical Society of America.

the results of the simulation for an integrating sphere of the Ulbricht type (one baffle and one window) are compared with those presented in previous papers. Then the window illuminances of the designed sphere models are computed for varying conditions such as the size and location of the baffles, openings, a test lamp, and the wall reflectance, and the calibration errors are analyzed. Finally one geometry of an integrating sphere that is most suitable for this purpose is proposed.

2. Sphere Geometry for a New Method of Total Flux Calibration

A. Requirements for the Geometry

The basic idea is to compare the total flux of a test lamp inside the sphere with the known flux coming into the sphere from a directionally calibrated standard lamp placed outside the sphere. To realize this method, an integrating sphere should be designed consisting of (1) a test lamp (internal source), (2) an observation window, (3) an opening to introduce flux from the standard lamp (external source), (4) a baffle between the test lamp and the observation window, and (5) a baffle between the test lamp and the opening to prevent the direct light of the test lamp from leaking out of the sphere.

Two basic models of an integrating sphere that meet these requirements have been designed. Figure 1 shows the geometry of the first model (Model 1) in which the opening is located 90° away from the observation window. Figure 2 shows the geometry of another model (Model 2) in which the opening is located farther from the detector. Neither of these models can be axially symmetric. In these models the input flux Φ_s can be determined by

$$\Phi_s = EA \quad (1\mathrm{m}), \tag{1}$$

where E is the average illuminance (lux) at the aperture plane, A is the area (square meters) of the aperture. Assuming the sphere throughput is constant, one obtains the total flux Φ_t of the test lamp by measuring the window illuminances for Φ_t compared with Φ_s.

Measurements are to be made in turn when only the test lamp is turned on and when only the external standard lamp is turned on and the detector readings in the two conditions are to be compared. There is no need for an auxiliary lamp to correct the self-

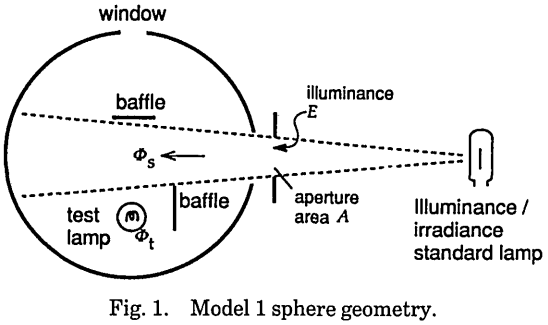

Fig. 1. Model 1 sphere geometry.

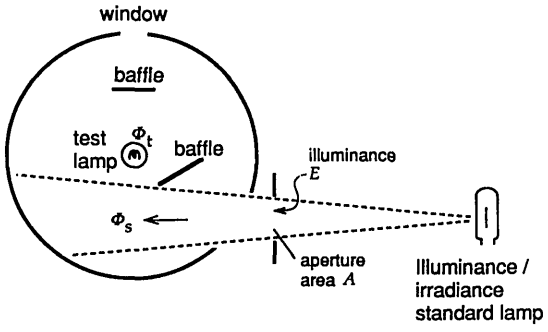

Fig. 2. Model 2 sphere geometry.

absorption of the test lamp, which is a requirement in the conventional substitution method, because the test lamp is kept in the same place inside the sphere when the measurement with the external source is made. There is also no need for another baffle between the observation window and the part of the sphere wall that is directly illuminated by the external source. In other words the detector must see the first reflection of the external source because the detector sees most of the first reflection of the test lamp; the number of interreflections in the two conditions must be balanced in this method. This requirement is different from many other applications in which the detector is usually not exposed to the directly illuminated area.

B. Sphere Geometry of the Simulation Model

Both Models 1 and 2 consist of the same objects; the only difference between the two models is the location and positioning of the objects. Therefore the equations and the algorithm for the computer-simulation program need to be derived for only one sphere geometry, which is shown in Fig. 3, in which a sphere of radius R with an observation window (radius R_d), internal source S_1, external source S_2, baffles B_1 and B_2, and an opening (radius R_0), is considered. Any point on the sphere wall is defined by the polar coordinate (θ, ϕ). Values D, D_1, and D_2 define the positions of baffle B_1 and baffle B_2. Angle β shows the tilt angle of baffle B_2. Angle α defines the position of the opening. The reflectances are defined as ρ_w for the sphere wall, ρ_d for the window and ρ_{b1u}, ρ_{b1L}, ρ_{b2r}, ρ_{b2L} for the surfaces of baffles B_1 and B_2. One can carry out simulations for either model by using the same program with a different set of input data (as discussed in Subsections 5.B and 5.C). One can also use the same program for the conventional Ulbricht-type sphere (as discussed in Subsection 5.A) by giving such input data as R_2 and R_0 as zero.

3. Basic Equations

A. Illuminance Distribution on the Sphere Surfaces

In this subsection all surfaces are assumed to be perfectly diffusing. The absorption and the reflection of light by the internal source are not considered. Illuminance on each baffle surface is assumed to be uniform over the area.

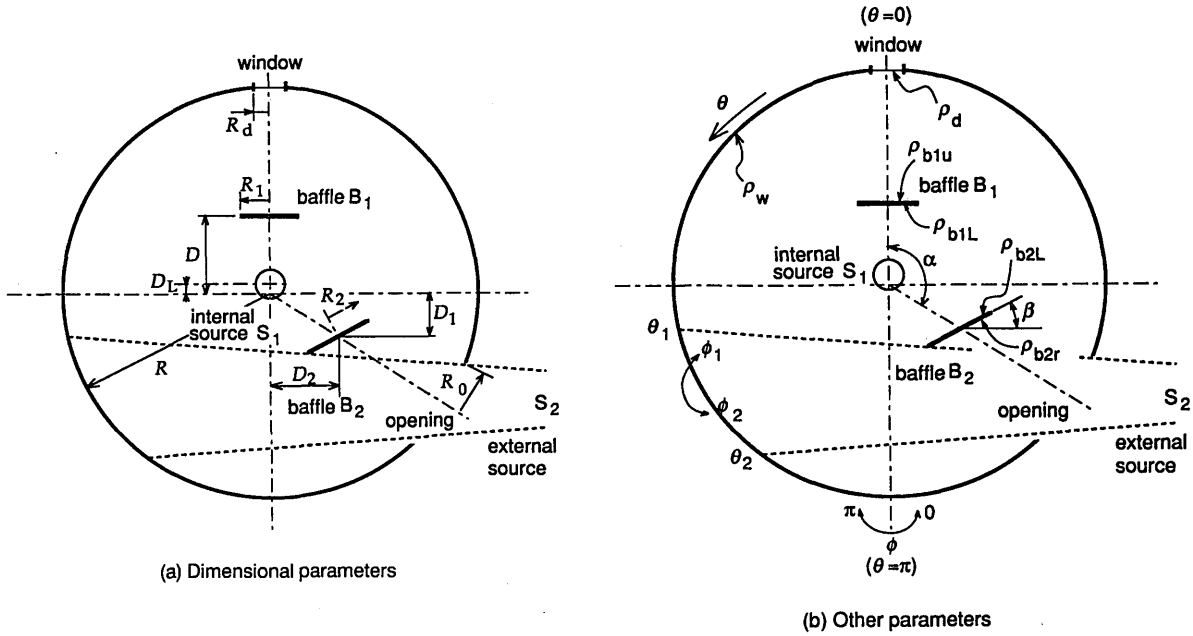

Fig. 3. Parameters for the computer model: (a) dimensional parameters, (b) other parameters.

Let us assume that W represents the surface of the sphere of Fig. 3 including the surfaces of baffles B_1 and B_2. Let $E_i(a)$ be the reflected illuminance on a given point a of W after the ith reflection and da be an area element of W. Then $E_i(a)$ is given by

$$E_i(a) = \frac{1}{\pi}\int\int_w \rho(a')E_{i-1}(a')S(a, a')T(a, a')\mathrm{d}a', \quad (2)$$

where $\rho(a)$ is the reflection factor at a, $S(a, a')$ is the screening factor whose value is either 1 or 0 depending on whether point a is seen from a'. $T(a, a')$ is the position factor that represents the distance factor between a and a' and the cosine factor of a and a'. On any point of the sphere wall, $T(a, a')$ is $1/(4R^2)$. Equation (2) is based on the equation of Brown[14] and de Visser and van der Woude[16] but is different in the way that the direct illuminance from either source is given as $E_0(a)$, and another direct illuminance is not considered until the reflected light by the first direct illuminance is totally absorbed. $E_0(a)$ is determined by the angular intensity distribution of the internal source or by the sphere geometry for introducing flux from outside. As shown in Eq. (2), $E_0(a)$ produces $E_1(a)$, and then $E_1(a)$ produces $E_2(a)$ and so on. The final illuminance distribution $E(a)$ on W is given by

$$E(a) = \sum_{i=0}^{\infty} E_i(a). \quad (3)$$

From this equation the final illuminance on any part of the sphere wall, including that on the observation window, which is our primary concern, can be obtained.

To solve Eq. (2) numerically, the surfaces of the baffles are separated from W, and Eq. (2) is redefined in terms of polar angle θ and azimuth angle ϕ as follows:

$$\begin{aligned} E_i(\theta, \phi) = \frac{1}{4\pi}\int_0^{2\pi}\int_0^{\pi} & E_{i-1}(\theta', \phi')\rho_w(\theta', \phi') \\ & \times S_{b1w}(\theta, \phi, \theta', \phi') \\ & \times S_{b2w}(\theta, \phi, \theta', \phi')\sin\theta'\mathrm{d}\theta'\mathrm{d}\phi' \\ & + \rho_{b1u}E_{i-1}(b1u)a_1T_{b1uw}(\theta, \phi)/\pi \\ & + \rho_{b1L}E_{i-1}(b1L)a_1T_{b1Lw}(\theta, \phi)S_{b2b1}(\theta, \phi)/\pi \\ & + \rho_{b2r}E_{i-1}(b2r)a_2T_{b2rw}(\theta, \phi)/\pi \\ & + \rho_{b2L}E_{i-1}(b2L)a_2T_{b2Lw}(\theta, \phi)S_{b1b2}(\theta, \phi)/\pi, \end{aligned} \quad (4)$$

$$\begin{aligned} E_i(b1u) = \frac{R^2}{\pi}\int_0^{2\pi}\int_0^{\pi} & E_{i-1}(\theta', \phi')\rho_w(\theta', \phi') \\ & \times T_{b1uw}(\theta', \phi')\sin\theta'\mathrm{d}\theta'\mathrm{d}\phi', \end{aligned} \quad (5)$$

$$\begin{aligned} E_i(b1L) = \frac{R^2}{\pi}\int_0^{2\pi}\int_0^{\pi} & E_{i-1}(\theta', \phi')\rho_w(\theta', \phi') \\ & \times S_{b2b1}(\theta', \phi')T_{b1Lw}(\theta', \phi')\sin\theta'\mathrm{d}\theta'\mathrm{d}\phi' \\ & + E_{i-1}(b2L)\rho_{b2L}a_2T_{b2b1}/\pi, \end{aligned} \quad (6)$$

$$\begin{aligned} E_i(b2r) = \frac{R^2}{\pi}\int_0^{2\pi}\int_0^{\pi} & E_{i-1}(\theta', \phi')\rho_w(\theta', \phi') \\ & \times T_{b2rw}(\theta', \phi')\sin\theta'\mathrm{d}\theta'\mathrm{d}\phi', \end{aligned} \quad (7)$$

$$\begin{aligned} E_i(b2L) = \frac{R^2}{\pi}\int_0^{2\pi}\int_0^{\pi} & E_{i-1}(\theta', \phi')\rho_w(\theta', \phi')S_{b1b2}(\theta, \phi) \\ & \times T_{b2Lw}(\theta', \phi')\sin\theta'\mathrm{d}\theta'\mathrm{d}\phi' \\ & + E_{i-1}(b1L)\rho_{b1L}a_1T_{b1b2}/\pi. \end{aligned} \quad (8)$$

$E_i(b1u)$, $E_i(b1L)$, $E_i(b2r)$, and $E_i(b2L)$ represent reflected illuminances after the ith reflection on the upper side of B_1, the lower side of B_1, the right side of B_2, and the left side of B_2, respectively. Only E_{b1L} and E_{b2L} consider the illuminance and the screening function of the other baffle because the two surfaces face each other. In these equations I do not consider the case where both surfaces of the baffle B_2 face part of baffle B_1. $S_{b1w}(\theta, \phi, \theta', \phi')$ is the screening function of B_1 seen from a point (θ, ϕ) on the wall, and $S_{b1b2}(\theta, \phi)$ is that of B_1 seen from B_2, a_1 and a_2 are the areas of one surface of B_1 and B_2, respectively; $\rho_w(\theta, \phi)$ is the reflectance of a point (θ, ϕ) on the wall including the window surface ρ_d and the opening (zero reflectance); ρ_{b1u}, ρ_{b1L}, ρ_{b2r}, ρ_{b2L} are the reflectances of each side of the baffles. $T_{b1uw}(\theta, \phi)$ is a function of the position factor between the upper surface of B_1 and a point (θ, ϕ) on the wall. The value of this function will be zero for a point (θ, ϕ), which is behind that surface of B_1. T_{b1b2} and T_{b2b1} are the position factors between B_1 and B_2, the two values being the same.

All these screening functions and position factor functions have been derived by geometrical calculations. The details of the derived equations are shown in Appendix A. I did all calculations assuming the illuminance on each surface of the baffles is uniform, and the illuminance on each side of the baffle is represented by the value on the geometrical center of the baffle surfaces.

B. Interreflection Window Illuminance Factor

Muroi[11] analyzed an integrating sphere with one baffle, introducing a factor $K(\theta, \phi)$ that determines the window illuminance from the flux of a sharp light beam incident only around point (θ, ϕ). The research of de Visser and van der Woude[16] was also based on the concept of this factor. In this paper $K(\theta, \phi)$ is called the interreflection window illuminance factor. One can analyze in detail the performance of any integrating sphere by looking into this factor. $K(\theta, \phi)$ can be calculated with Eq. (3) as follows:

$$K(\theta, \phi) = \sum_{i=0}^{\infty} E_i(0, 0)/\Phi_b \quad (\mathrm{lx/lm}), \tag{9}$$

where $E_0(\theta', \phi') = \Phi_b/\mathrm{d}a$ at (θ, ϕ), and $E_0(\theta', \phi') = 0$ at another part of the sphere wall, $\mathrm{d}a$ being the area of the element on which the beam is incident and Φ_b the beam flux. A light source with any angular intensity distribution $I(\theta, \phi)$ can be considered to consist of a large number of such sharp beams. The window illuminance E_w is then

$$E_w = \int_0^{2\pi} \int_0^{\pi} K(\theta, \phi) I(\theta, \phi) \sin\theta \mathrm{d}\theta \mathrm{d}\phi. \tag{10}$$

This equation means that if $K(\theta, \phi)$ is constant, E_w is perfectly proportional to the total flux of the light source, whatever $I(\theta, \phi)$ may be. For an ideal sphere $K(\theta, \phi)$ is equal to $\rho_w/[4\pi R^2(1 - \rho_x)]$, where ρ_w is the wall reflectance and ρ_x is the average reflectance of the sphere surfaces including the window and the opening. Any variation of values of $K(\theta, \phi)$ causes errors associated with the angular intensity distribution of the source.

4. Computer-Simulation Model

A. Approach

The approach of this computer simulation is basically to compute Eqs. (3)–(8) numerically. Because of the lack of axial symmetry, the sphere is divided into many small sections defined by θ and ϕ. One calculates the illuminance of each section one reflection after another by totaling the illuminances produced by all the sections of the sphere surfaces including each surface of B_1 and B_2, taking the screening functions of B_1 and B_2 into account as described in Subsection 3.A.

The determination of the number N_s of sections to be divided into is a compromise between the accuracy of the simulation and the calculation time. This simulation is a heavy load even for a high-speed computer, and also the calculation time is proportional to N_s^2. Therefore N_s should not be chosen to be too large. If N_s is too small, on the other hand, the areas of the window or the opening may not be adjusted well enough to the specified values because several sections are grouped together to be the window or the opening. In our model the steps of $10° \times 5°$ and $5° \times 5°$ $(\theta \times \phi)$ were tested, and $10° \times 5°$ steps were finally chosen because there was no significant difference in the results for the two conditions. The window illuminance is calculated as the mean value of the illuminance on the window sections.

B. Errors Associated with the Finite Number of Reflections

Calculations of Eqs. (3)–(8) should be iterated until the unabsorbed flux is small enough to be neglected. I discuss here how many iterations are necessary. Based on the first-order calculation, assuming that the reflectance on the sphere wall is uniform, the total flux $\Phi_{tot}(n)$ inside the sphere after the nth reflection is

$$\phi_{tot}(n) = \phi_{in}\left(1 + \rho_w \sum_{i=1}^{n} \rho_x^{\,i-1}\right) \qquad (n \geq 1), \tag{11}$$

where ϕ_{in} is the initial input flux, ρ_w is the wall reflectance, and ρ_x is the average reflectance of the sphere wall including the opening. The unabsorbed flux after the nth reflection, on the other hand, is

$$\phi_{un}(n) = \phi_{in}\rho_w\rho_x^{\,n-1} \qquad (n \geq 2). \tag{12}$$

Considering that the initial flux ϕ_{in} does not contrib-

ute to the detector signal, one derives the relative calculation error $\epsilon(n)$ caused by the abortion of calculation at the nth reflection from Eqs. (11) and (12) and is

$$\epsilon(n) = \frac{\phi_{tot}(\infty) - \phi_{tot}(n)}{\phi_{tot}(\infty) - \phi_{in}} = \rho_X n \simeq \frac{\Phi_{un}(n)}{\phi_{in}}. \quad (13)$$

Figure 4 shows the plots of Eqs. (11) and (12) in which the relation of Eq. (13) is obviously seen. In our model aborting error ϵ_a is first specified and $\epsilon(n)$ is calculated after each reflection. When $\epsilon(n)$ becomes smaller than ϵ_a, the calculation automatically stops. In this manner one controls the number of iterations, depending on ρ_x and other effects, keeping the accuracy constant. For absolute comparison the results can be corrected by ϵ_a since they should be lower by ϵ_a than the true values. In relative comparison, ϵ_a need not be very small, e.g., ϵ_a of 0.05 results in 5% lower absolute values, but in relative comparison the errors were found to be less than 0.02% (in Model 2). In the simulations in Subsections 5.B and 5.C, 0.05 is used for ϵ_a, and the number of iterations is kept constant among the data compared.

C. Sampling Errors

When the illuminance $E(\theta, \phi)$ on section (θ, ϕ) from section $(\theta'\phi')$ is calculated, the screening function $S(\theta, \phi, \theta', \phi')$ is calculated to be either 1 or 0, depending on the geometry of the centers of each section, even though the section may be only partially screened by the baffle. Calculating true values between 1 and 0 would be too complicated and not realistic for this computer model, which means that illuminance can be overestimated from some sections and underestimated from others. If the total of overestimation and underestimation is not balanced, there is some error. This error hereafter is called a sampling error. Before this problem was in consideration in the program, it was experienced that the calculated window illuminance values scattered ±0.3% at maximum with a small change of baffle parameters, which was not acceptable.

To solve this problem, a new algorithm was adopted in which, when $S(\theta, \phi, \theta'\theta')$ is 1 (not screened) the luminance $L(\theta', \phi')$ on the wall is taken, and when $S(\theta, \phi, \theta'\phi')$ is 0 (screened) the luminance of the particular baffle surface (instead of 0) is taken to calculate $E(\theta, \phi, \theta', \phi')$; i.e., the illuminance from the baffle surface, which was calculated separately in the old algorithm, is also calculated at the same time. This idea is based on the relation that the illuminance E_p on point P produced by the luminance L_s on a surface S at distance d is

$$E_p = L_s s, \quad (14)$$

where s is the solid angle subtended by surface S from point P, which means that E_p does not depend on the distance d and/or the angle of surface S provided that the solid angle s is constant and surface S is a perfect diffuser. With this improved algorithm, adopted in our computer model, although the equivalent size of the baffle may be varied slightly, the sampling errors were reduced to a negligible level.

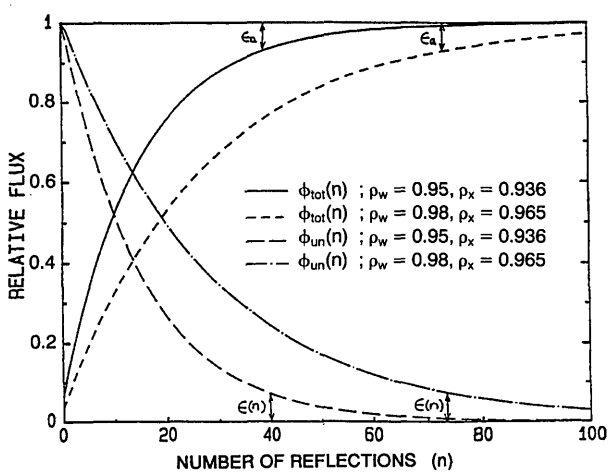

Fig. 4. Total flux $\Phi_{tot}(n)$ and unabsorbed flux $\Phi_{un}(n)$ as a function of the number of reflections n. The data are normalized by the maximum value for each curve.

D. Initial Illuminance Distribution

For the internal source a point source with uniform intensity distribution was assumed. The initial illuminance distribution is calculated from the luminous intensity of the source that is calculated by the specified total flux value of the source, with the screening functions of baffles taken into account as shown in Appendix B for detail. However, when the total flux incident on all the sphere sections plus baffle surfaces is calculated from the calculated illuminance values, it does not agree perfectly with the given total flux of the source. This disagreement is caused by sampling errors. Therefore the illuminance distribution is rescaled to make the total flux incident on the sphere surfaces equal to the total flux of the source.

For the external source the illuminated part is specified by the range of θ and ϕ, depending on the geometry of the opening and the external source, and the initial illuminance on this part is calculated from the area of that part and the total flux value specified. In this way the input total flux from either source is kept exactly the same. All the simulations shown in Section 5 used the input total flux value of 1 (lm) except for one shown in Fig. 5.

In addition to an internal source with uniform intensity distribution, I prepared several variations of the intensity distribution by excluding incident light on some part of the sphere surface to evaluate the

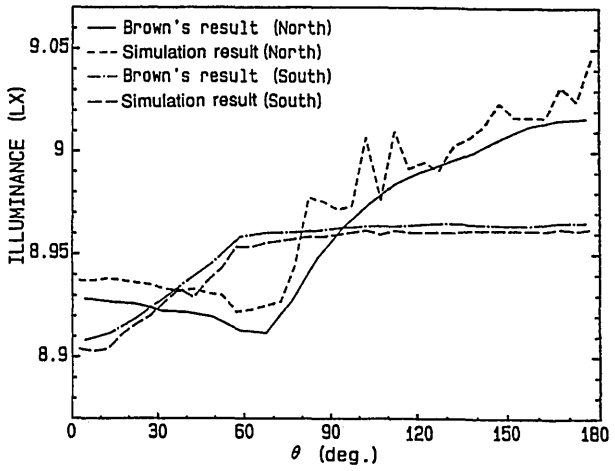

Fig. 5. Comparison of the simulation results of the illuminance distributions on the sphere wall with Brown's results by using Brown's parameters. North and South refer only to lighting the upper or lower hemisphere, respectively. Parameter $R = 1.0$, $R_d = 0, R_0 = 0, R_1 = 0.1, R_2 = 0, D = 0.31, D_L = 0$, ρ on all surfaces are 0.90.

effects of baffles or the errors caused by different intensity distributions of the internal source.

E. Consideration of Calculation Time

The first integration of Eq. (4) is the dominant element of the entire simulation in terms of calculation time. This integration takes 2592 (for 5° × 5° steps) calculations of the two screening functions and multiplication of $E_{i-1}(\theta, \phi)$ and $\rho(\theta, \phi)$. To obtain the distribution over the sphere surface, the same calculation must be repeated 6,718,464 times for each reflection. When the multiple interreflections are considered, an enormous number of calculations are expected. Therefore the following algorithm was adopted to reduce calculation time as much as possible.

(1) Utilizing the plane symmetry of the sphere geometry reduces the calculation time by half.

(2) The screening functions are calculated before the main calculation and stored in a large bit array. This array takes a large memory capacity, but the calculation time is reduced by a factor of more than 10 compared with the procedure where the screening function is calculated at each path.

The computer simulation program was written in Fortran, and it was run on a super computer CDC Cyber 205 at National Institute of Standards and Technology, Gaithersburg, Md. With the Fortran program vectorized, it took ~30 s (CPU time) to compute one condition with 10° × 5° steps with 100 interreflections. On a 20-MIPS (million instructions per second) UNIX machine the same computation took ~30 min.

5. Results

A. Ulbricht-Type Sphere

To verify the simulation program, an integrating sphere of the Ulbricht type (the geometry used in ordinary sphere photometers) was simulated in the same conditions as used in the studies of Brown[14] and de Visser and van der Woude.[16] First, I performed simulations to repeat Brown's calculation. The distribution of the indirect illuminance on the wall obtained by the simulation is shown in Fig. 5 compared with Brown's results. Although slight sampling errors are recognized in the North curve, the two results are in good agreement. The simulation used an aborting error value ϵ_a of 0.01 (refer to Subsection 4.B), and all the results were corrected by that factor.

Next a series of simulations was made to obtain the interreflection window illuminance factor $K(\theta, \phi)$ of a sphere with the parameters used in de Visser and van der Woude's calculation. Figure 6 shows the results of the simulation compared with de Visser and van der Woude's results. The two curves are also in very good agreement.

These results show that the extension of this simulation to include a more complex design including two baffles is valid.

B. Model 1-Type Sphere

The basic set of parameters for Model 1 (Fig. 1) was chosen for an opening size 12.7 cm in diameter on a sphere 50.8 cm in diameter, which is the size of a sphere that is planned to be used for the following experimental analysis. Experiments are planned to calibrate the total flux of miniature lamps (6–400 lm) against the flux (~20 lm) introduced from a 1-kW quartz halogen spectral irradiance standard lamp at 0.5 m away from the opening. The size and location of the baffles were determined for an internal source

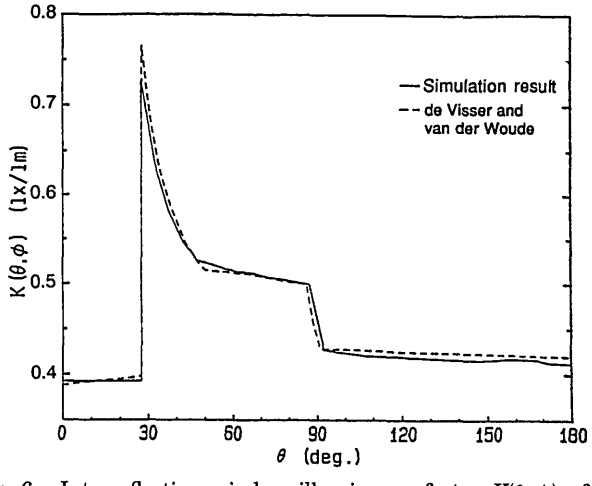

Fig. 6. Interreflection window illuminance factor $K(\theta, \phi)$ of a sphere with parameters used in de Visser and van der Woude's calculation. Parameters $R = 1.0, R_d = 0, R_0 = 0, R_1 = 0.348, R_2 = 0, D = 0.663, D_L = 0$, $\rho_w = \rho_{b1u} = \rho_{b1L} = 0.90$.

of 4-cm maximum diameter and a window 4 cm in diameter. Other basic parameters are shown in Table 1.

Table 1 shows a comparison of the window illuminances obtained with the internal source E_{w1} versus the external source E_{w2} with one of the parameters varied. For all the results E_{w1} is lower than E_{w2}. The difference $(E_{w1} - E_{w2})$ becomes smaller for the increasing wall reflectance as well as for the decreasing baffle B_1 size R_1. The result at the bottom of the table is for an imaginary condition in which the opening and baffle B_2 are eliminated. Figure 7 shows the variation of window illuminances, E_{w1} and E_{w2}, for the internal and external sources, respectively, as a function of distance D for baffle B_1 from the sphere center. This result shows that baffle B_1 in this model should be placed as close as possible to the sphere center.

Figure 8 shows a plot of the calculated curves of $K(\theta, \phi)$ at $\phi = 0$ and $\phi = 180°$. Both curves are normalized by the value of E_{w2} of this model. Note that (θ, ϕ) in this figure designates the direction of the beam from the light source, which is located off the sphere center. In this curve the effects of baffles and openings are clearly visible. Figure 8 shows the lower surface of B_1 [1], the left-hand surface of B_2 [2], the part screened by baffle B_2 (from the window) [3], and the part screened by baffle B_1 [4]. $K(\theta, \phi)$ is significantly lower in thse regions because the reflection from these areas cannot or can hardly reach the window directly. Such a decrease of $K(\theta, \phi)$ should be taken into account for the internal source, whereas for the external source only the value at area [5] is effective. From these results it is concluded that the sources of error for the significant differences in the results of Table 1 are as follows:

(1) The internal source is placed near the bottom of the sphere, and a large portion of radiation is incident on the area where $K(\theta, \phi)$ is lower.

(2) Baffle B_2 is positioned almost normal to the direction of the window, which makes $K(\theta, \phi)$ of this surface lower.

Table 1. Comparison of Calculated Window Illuminance for Model 1[a]

Varied Parameter	E_{w2} (lx)	E_{w1} (lx)	Difference (%)
$\rho = 0.90$	9.168	9.046	−1.33
$\rho = 0.95$	17.119	17.003	−0.68
$\rho = 0.98$	32.575	32.484	−0.29
$R_1 = 0.02$	17.119	17.003	−0.68
$R_1 = 0.03$	17.053	16.850	−1.19
$R_1 = 0.04$	16.960	16.649	−1.83
$R_2 = R_0 = 0$	21.436	21.759	−0.39

[a] E_{w1} is for the internal source, E_{w2} is for the external source. Basic parameters $R = 0.254$, $R_d = 0.02$, $R_0 = 0.06$, $\alpha = 90°$, $D_L = 0.15$, $R_1 = 0.02$, $D = 0.09$, $R_2 = 0.04$, $D_1 = 0.11$, $D_2 = 0.07$, $\beta = 90°$, $\theta_1 = 70°$, $\theta_2 = 110°$, $\phi_1 = 160°$, $\phi_2 = 200°$, $\rho_w = 0.95$, ρ on baffles $= 0.95$, $\epsilon_a = 0.05$.

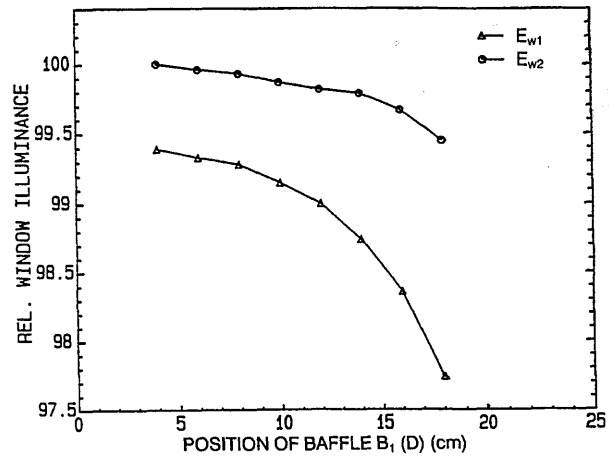

Fig. 7. Window illuminance as a function of the location D of baffle B_1 on Model 1 with basic parameters.

C. Model 2-Type Sphere

Based on the results obtained for Model 1, the sphere geometry was modified and Model 2 (Fig. 2) was designed. Parameters R, R_d, R_0, R_1 were kept the same as those in Model 1. It was expected that one would minimize factor (1) by placing the internal source in the sphere center and improve factor (2) by placing the opening farther down so that the irradiated surface of B_2 may face the detector better. It was also expected that, by tuning the angle β of B_2, one might balance the sphere efficiency for the internal source and for the external source.

The results of Model 2 with the basic parameters are shown in Fig. 9. The graph shows the window illuminance E_{w1}, E_{w2} (solid curves) and the total flux Φ_{tot1}, Φ_{tot2} (dashed curves) for the internal and external sources, respectively, as a function of the angle β of baffle B_2. Both illuminance and flux values are normalized by the values obtained with the external source with $\beta = 20°$. A value of 0.95 was used for the reflectance of the wall and all baffle surfaces. In this

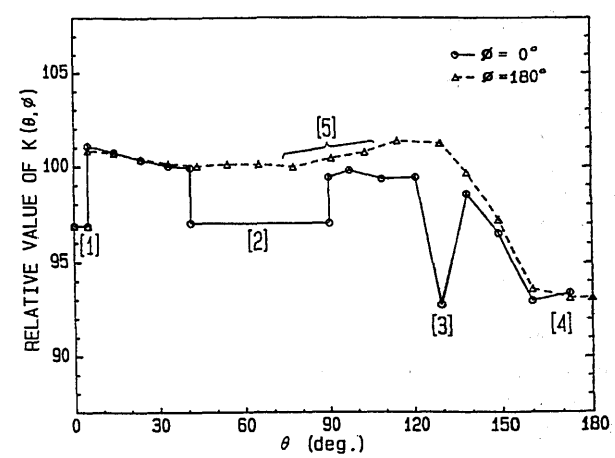

Fig. 8. Interreflection window illuminance factor $K(\theta, \phi)$ of Model 1 with basic parameters as a function of direction θ from the internal source.

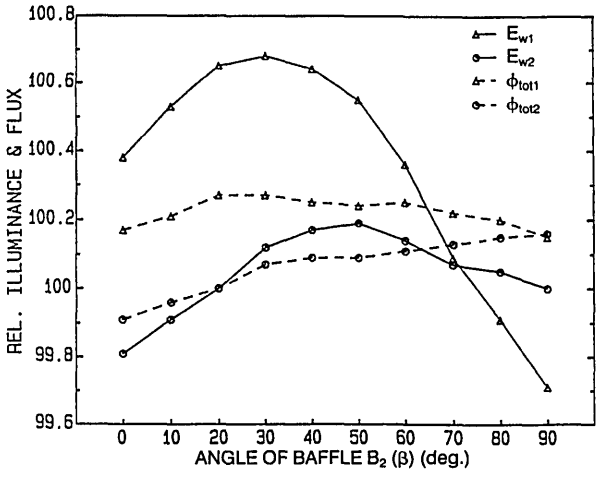

Fig. 9. Window illuminance and total flux by the internal source (E_{w1}, Φ_{tot1}), and by the external source (E_{w2}, Φ_{tot2}) as a function of the angle β of baffle B_2 on Model 2. Parameters $R = 0.254$, $R_d = 0.02$, $R_0 = 0.06$, $\alpha = 130°$, $R_1 = 0.02$, $D = 0.09$, $D_L = 0$, $R_2 = 0.045$, $D_1 = 0.059$, $D_2 = 0.07$, $\theta_1 = 110°$, $\theta_2 = 150°$, $\epsilon_a = 0.05$, ρ on all surfaces is 0.95.

graph E_{w1} and E_{w2} are balanced near $\beta = 70°$ as expected. The falloff in the flux curves for smaller values of β indicates decreasing sphere efficiency, which seems to affect the illuminance curves as well. The falloff of the window illuminance for larger values of β is considered to be caused partly by the screening effect of B_2 between the detector window and the opening. (Part of the opening is seen from the window.) To analyze this further, I calculated the window illuminance for different direct-illuminance distributions. Figure 10 shows the results for illuminances, which are (1) uniform, (2) uniform but not incident on B_2, (3) incident only on B_2, (4) with the external source. From this graph we see that curve (2) is similar to curve (4) and curve (3) is similar to curve (1). From this observation one finds that the difference between E_{w1} and E_{w2} is caused largely by the direct illuminance on B_2. In response, B_2 should

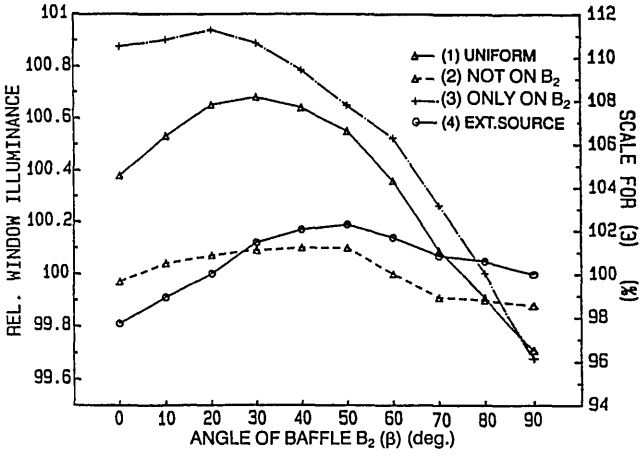

Fig. 10. Window illuminance by different direct illuminance distributions as a function of β on Model 2.

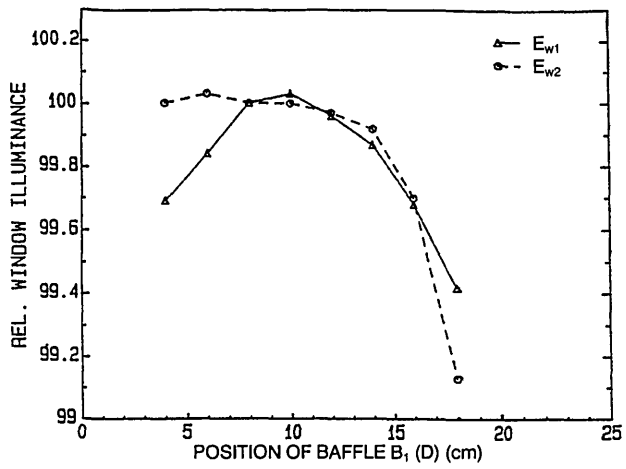

Fig. 11. Window illuminance by the internal source E_{w1} and by the external source E_{w2} as a function of the location D of baffle B_1 on Model 2.

be located as far as possible from the source (or window) and made as small as possible, although the geometry is restricted by the size and location of the opening.

As for the location of baffle B_1, $D = 9$ cm (nearly one-third of R) was chosen as a basic parameter, which is considered theoretically to minimize the effect of B_1.[11,14] To verify this, simulations were performed, varying the value of D. Figure 11 shows the window illuminance E_{w1} (internal source) and E_{w2} (external source) as a function of D with β fixed at 70°. Values are normalized by the value of E_{w2} at $D = 4$ cm. The peak of each curve is considered to be the point where the effect of B_1 is minimum. The curve for the internal source has its peak at around one-third to two-fifths of R, which is in perfect agreement with the theory. The graph also indicates that E_{w2} is not affected by D as long as B_1 is not too close to the window.

In Fig. 12 the window-illuminance curves for differ-

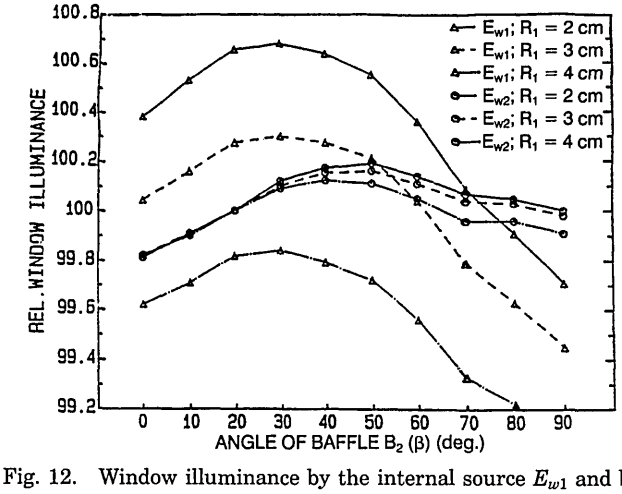

Fig. 12. Window illuminance by the internal source E_{w1} and by the external source E_{w2} as a function of the angle β of baffle B_2 on Model 2 with different sizes (radius R_1) of baffle B_1.

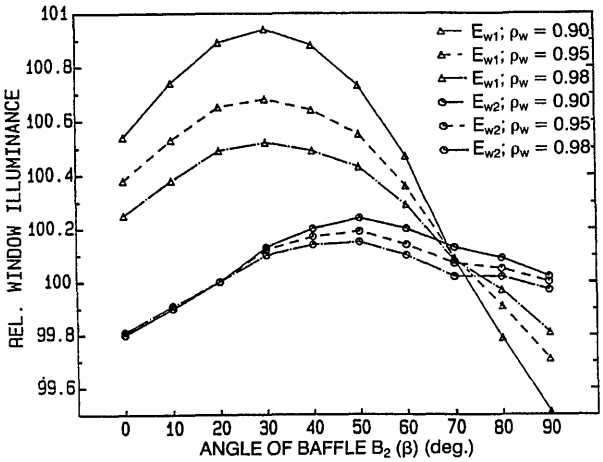

Fig. 13. Window illuminance by the internal source E_{w1} and by the external source E_{w2} with different wall reflectances ρ_w.

ent sizes of B_1 (R_1) are shown. One finds that changing R_1 shifts only the E_{w1} curve, resulting in a shift of the balancing point, i.e., the optimum value for β depends on R_1.

In Fig. 13 the window-illuminance curves for different wall reflectances are compared. The same reflectance values are used for baffle surfaces. It is clear from this result that the higher the reflectance is, the smaller the effect of the baffle angle. (Wavelength selectivity is not considered here.) However, note that the change of ρ_w does not affect the balancing point much; i.e., even when the reflectance is low the error can still be controlled to be small enough if β is chosen correctly. It was also found by another simulation that changing only ρ_{b2L} (reflectance of the left surface of B_2) shifts the balancing point significantly.

The errors associated with the intensity distribution of the internal source were evaluated by simulation with (1) the uniform intensity for all angles, (2) the uniform intensity toward only the upper hemisphere, and (3) the uniform intensity toward only the lower hemisphere. The results are shown in Fig. 14 where curve (4) represents the external source case. This result shows that the errors caused by different intensity distributions of the internal source are not serious near the balancing point. It is also possible to evaluate and correct errors with intensity distributions $I(\theta, \phi)$ of real sources.

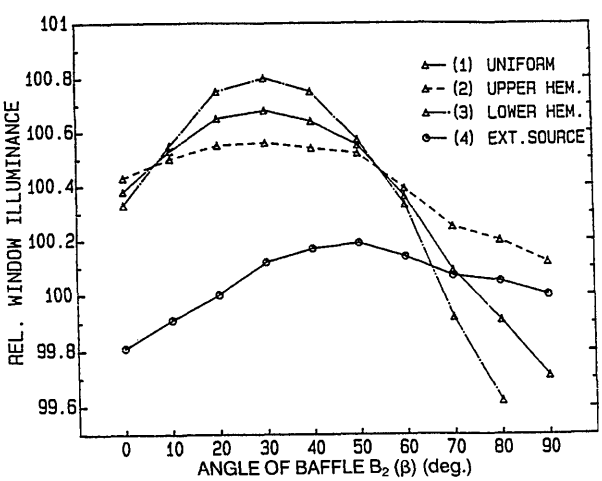

Fig. 14. Window illuminance curves with different intensity distributions of the internal source.

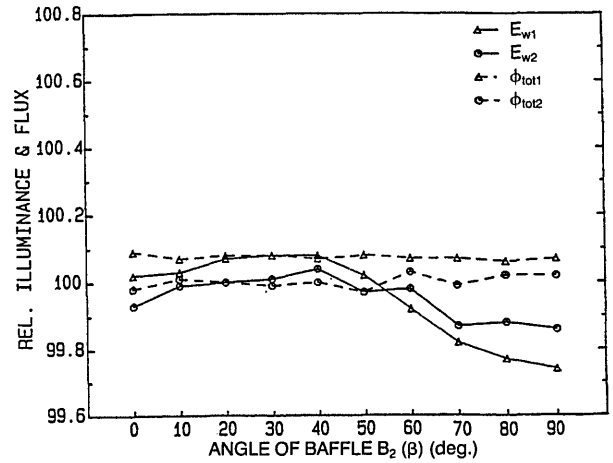

Fig. 15. Window illuminance and total flux on Model 2 with smaller opening and smaller baffle B_2. Parameters $R_0 = 0.045$, $R_2 = 0.038$, $D_1 = 0.084$, $D_2 = 0.10$, $\theta_1 = 115°$, $\theta_2 = 145°$. (Other parameters are as in Fig. 9.)

Another simulation was made with a sphere of the same size with a different size opening (9 cm in diameter). Baffle B_2 is also smaller and placed closer to the opening. Figure 15 shows the results for this geometry. Other parameter values are in the figure caption. Although there are some sampling errors, the results show that the calibration error with this geometry is less than 0.1% regardless of β. All other errors are also assumed to be much smaller than those for the case of the larger opening.

6. Summary and Conclusion

Two models of an integrating sphere with an opening and a pair of baffles were designed for a new method of realizing the total flux scale. A computer simulation program was developed to analyze the sphere models and to predict the calibration accuracy. Equations were derived for the sphere geometry to be applied for the ray-tracing technique. To realize sufficient accuracy for radiometric purposes, an algorithm was developed in the program that minimizes the sampling errors. The simulation results were verified compared with analyses reported in the past on a sphere of simple geometry. Simulations were carried out with many variations of sphere geometry, and it was shown that one of the models would have sufficient accuracy for practical use of this method. It was shown that one could balance the sphere efficiency for the internal source with that for the external source by selecting the position and the angle of the baffles appropriately. It was also shown that a higher reflectance of the sphere wall makes the

sphere design less critical. The calibration errors even with different intensity distributions of the internal source were predicted to be within a few tenths of a percent. Although this simulation was intended for the particular sphere models, the equations and the algorithm can be applied generally to the integrating spheres of other geometries.

The models were designed assuming an actual experimental setup for calibrating the total flux of miniature lamps. However, this method can be applied to larger spheres for ordinary lamps. In that case the opening is much smaller relative to the sphere size, and the systematic errors can be even smaller than reported here. This method can also be applied in principle to establish the spectral total radiant flux scale. In such cases the experimental aspects of the linearity and the detectivity of detectors or monochromators may be important, because the illuminance or the spectral irradiance at the detector window of larger spheres is at a significantly low level for the external source.

In the simulation many other factors, such as the reflectance nonuniformity over the sphere wall, the reflection properties of the sphere coating, and the detector's angular response variation, were not considered. To verify the accuracy of this calibration method further, and also the accuracy of the computer simulation, an experimental verification is necessary.

The author thanks D. A. McSparron and K. D. Mielenz for their discussions and guidance.

Appendix A: Screening Functions and Position Factor Functions of Baffles

The variables used in this Appendix are specified in Fig. 3 unless given in particular. For convenience in deriving the equations the restrictions of $D > -D_1$, $D_2 \geq 0, D_L < D$ are assumed.

Consider two points (θ, ϕ) and (θ', ϕ') on the sphere surface. When the (θ, ϕ) coordinate is changed into the (x, y, z) coordinate, the two points are expressed:

$$x_1 = R \sin \theta_1 \sin \phi_1,$$
$$y_1 = R \sin \theta_1 \cos \phi_1,$$
$$z_1 = R \cos \theta_1, \tag{A1}$$

$$x_2 = R \sin \theta_2 \sin \phi_2,$$
$$y_2 = R \sin \theta_2 \cos \phi_2,$$
$$z_2 = R \cos \theta_2. \tag{A2}$$

The screening function $S_{b1w}(\theta_1, \phi_1, \theta_2, \phi_2)$ of baffle B_1 between point (θ_1, ϕ_1) and point (θ_2, ϕ_2) is

$$S_{b1w}(\theta_1, \phi_1, \theta_2, \phi_2) = 1 \text{ for } x_0^2 + y_0^2 > R_1^2$$
$$= 0 \text{ for } x_0^2 + y_0^2 \leq R_1^2, \tag{A3}$$

where

$$x_0 = (D - z_1)(x_2 - x_1)/(z_2 - z_1) + x_1,$$
$$y_0 = (D - z_1)(y_2 - y_1)/(z_2 - z_1) + y_1.$$

The screening function $S_{b2w}(\theta_1, \phi_1, \theta_2, \phi_2)$ of baffle B_2 between points (θ_1, ϕ_1) and (θ_2, ϕ_2) is

$$S_{b2w}(\theta_1, \phi_1, \theta_2, \phi_2)$$
$$= 1 \text{ for } x_0^2 + (y_0 - D_2)^2 + (z_0 + D_1)^2 > R_2^2$$
$$= 0 \text{ for } x_0^2 + (y_0 - D_2)^2 + (z_0 + D_1)^2 \leq R_2^2, \tag{A4}$$

where

$$x_0 = x_1 + (x_2 - x_1)(y_0 - y_1)/(y_2 - y_1),$$
$$y_0 = \frac{(k - nz_1)(y_2 - y_1) + ny_1(z_2 - z_1)}{m(y_2 - y_1) + n(z_2 - z_1)},$$
$$z_0 = \frac{(k - my_1)(z_2 - z_1) + mz_1(y_2 - y_1)}{n(z_2 - z_1) + m(y_2 - y_1)},$$

where

$$k = [D_1(D_1 + D_3) + D_2^2][(D_1 + D_3)^2 + D_2^2]^{-1/2},$$
$$m = D_2[(D_1 + D_3)^2 + D_2^2]^{-1/2},$$
$$n = -(D_1 + D_3)[(D_1 + D_3)^2 + D_2^2]^{-1/2},$$

where k, m, n are the constants for the equation of the plane including the baffle B_2 as given by

$$my + nz = k.$$

D_3 is the y intercept of a perpendicular of baffle B_2 from the center of B_2 as given by

$$D_3 = D_2/\tan \beta - D_1.$$

The position factors $T_{b1uw}(\theta, \phi)$ and $T_{b1Lw}(\theta, \phi)$ between the upper and lower surfaces of baffle B_1 and point (θ, ϕ) are

$$f(\theta, \phi) = \frac{|D - R \cos \theta|\,(R - D \cos \theta)}{(R^2 + D^2 - 2RD \cos \theta)^2},$$

$$T_{b1uw}(\theta, \phi) = f(\theta, \phi) \quad \text{for } D < R \cos \theta$$
$$= 0 \quad \text{for } D \geq R \cos \theta, \tag{A5}$$

$$T_{b1Lw}(\theta, \phi) = 0 \quad \text{for } D < R \cos \theta$$
$$= f(\theta, \phi) \quad \text{for } D \geq R \cos \theta. \tag{A6}$$

The position factors $T_{b2rw}(\theta, \phi)$ and $T_{b2Lw}(\theta, \phi)$between the right and left surfaces of baffle B_2 and point (θ, ϕ) are

$$f(\theta, \phi) = \frac{[(y_1 - y_0)^2 + (z_1 - z_0)^2]^{1/2}(R + D_1 \cos\theta - D_2 \cos\phi \sin\theta)}{[R^2 + D_1{}^2 + D_2{}^2 + 2R(D_1 \cos\theta - D_2 \sin\theta \cos\phi)]^2},$$

$$\begin{aligned} T_{b2rw}(\theta, \phi) &= f(\theta, \phi) && \text{for } my_1 + nz_1 > k \\ &= 0 && \text{for } my_1 + nz_1 \le k, \end{aligned} \tag{A7}$$

$$\begin{aligned} T_{b2Lw}(\theta, \phi) &= 0 && \text{for } my_1 + nz_1 > k \\ &= f(\theta, \phi) && \text{for } my_1 + nz_1 \le k. \end{aligned} \tag{A8}$$

The screening function $S_{b2b1}(\theta, \phi)$ of baffle B_2 between baffle B_1 and point (θ, ϕ) is expressed by Eq. (A4) in which $x^2 = 0$, $y_2 = 0$, $z_2 = D_L$. The screening function $S_{b1b2}(\theta, \phi)$ of baffle B_1 between baffle B_2 and point (θ, ϕ) is expressed by Eq. (A3) in which $x_2 = 0$, $y_2 = D_2$, $z_2 = -D_1$. The positioning factors T_{b1b2} and T_{b2b1} are given by

$$T_{b1b2} = \frac{(D + D_1)[D_2{}^2 + (D_1 + D)(D_1 + D_3)]}{[(D + D_1)^2 + D_2{}^2]^2[(D_3 + D_1)^2 + D_2{}^2]^{1/2}},$$

$$T_{b2b1} = T_{b1b2}. \tag{A9}$$

Appendix B: Initial-Illuminance Distribution

The initial-illuminance distribution $E_0(\theta, \phi)$ on the sphere wall is given by

$$E_0(\theta, \phi) = \frac{I(\theta, \phi)(R - D_L \cos\theta)S_{b1s}(\theta, \phi)S_{b2s}(\theta, \phi)}{(R^2 + D_L{}^2 - 2RD_L \cos\theta)^{3/2}}, \tag{B1}$$

where $S_{b1s}(\theta, \phi)$ is expressed by Eq. (A3) in which $x_2 = 0, y_2 = 0, z_2 = D_L$. $S_{b2s}(\theta, \phi)$ is expressed by Eq. (A4) in which $x_2 = 0, y_2 = 0, z_2 = D_L$. The condition $z_1 > 0$ for $S_{b1s}(\theta, \phi) = 1$ and $y_1 > 0$ for $S_{b2s}(\theta, \phi) = 1$ should be added, because otherwise an image of the baffle appears in the opposite direction in the sphere.

The initial illuminance on baffles $E_0(b1L)$ and $E_0(b2L)$ are given by

$$E_0(b1L) = I(0, 0)/(D - D_L)^2, \tag{B2}$$

$$E_0(b2L) = \frac{I(\alpha, 0)[D_2{}^2 + (D_1 + D_3)(D_1 + D_L)]}{[(D_1 + D_L)^2 + D_2{}^2]^{3/2}[(D_1 + D_3)^2 + D_2{}^2]^{1/2}}. \tag{B3}$$

References

1. J. Bastie, B. Andasse, and R. Foucart, "Luminous flux measurements with a goniophotometer; study of time effects on data collection," in *Proceedings of the 22nd Session of the International Commission on Illumination* (Commission Internationale de l'Eclairage, Vienna 1991), Vol. 1 (1), Div. 2, pp. 45–47.
2. R. S. Hu, "Importance of axis alignment in goniophotometry," in *Proceedings of the 22nd Session of the International Commission on Illumination* (Commission Internationale de l'Eclairage, Vienna 1991), Vol. 1 (1), Div. 2, pp. 21–22.
3. I. Lewin, R. Laird, and B. Carruthers, "Development of new photometer concepts for quality control applications," J. Illum. Eng. Soc. **19,** (2), 90–97 (1990).
4. R. E. Levin, "Photometric connection," Light Des. Appl. **12**(9), 28–35 (1982).
5. T. Otsuka, H. Hatanaka, T. Sakaguchi, M. Fukuhara, and T. Noguchi, "A study on the photometric measurement of floodlights," in *Proceedings of the 22nd Session of the International Commission on Illumination* (Commission Internationale de l'Eclairage, Vienna 1991), Vol. 1 (1), Div. 2, pp. 3–4.
6. T. M. Goodman, J. R. Moore, N. C. Pearce, and D. K. Murray, "The establishment of a new national scale of spectral total flux," in *Proceedings of the 22nd Session of the International Commission on Illumination* (Commission Internationale de l'Eclairage, Vienna 1991), Vol. 1 (1), Div. 2, pp. 50–53.
7. J. Jacquez and H. Kuppenheim, "Theory of the integrating sphere," J. Opt. Soc. Am. **45,** 460–470 (1955).
8. D. Goebel, "Generalized integrating-sphere theory," Appl. Opt. **6,** 125–128 (1967).
9. M. Finkel, "Integrating sphere theory," Opt. Commun. **2,** 25–28 (1970).
10. E. Evans and S. Lowenthal, "Moment generator: new role for the integrating sphere," J. Opt. Soc. Am. **62,** 411–415 (1972).
11. T. Muroi, "Investigation on the luminous flux integration by closed space," J. Illum. Eng. Inst. Jpn. **43,** 52–57 (1959).
12. L. Morren, "Method for assessing the effect of the screen in an integrating sphere with an application to the photometry of a tubular lamp," Appl. Opt. **10,** 2621–2628 (1971).
13. F. Rotter, "View into the integrating sphere through the observation window," Appl. Opt. **10,** 2629–2638 (1971).
14. R. Brown, "A numerical solution of the integral equation describing a photometric integrating sphere," J. Res. Natl. Bur. Stand. Sect. A **77,** 343–351 (1973).
15. W. Fussel, "Approximate theory of the photometric integrating sphere," Natl. Bur. Stand. (U.S.) Tech. Note 594-7 (1974).
16. A. C. M. de Visser and M. van der Woude, "Minimization of the screen effect in the integrating sphere by cariation," Light. Res. Technol. **12,** 42–49 (1980).